Chapter 5
Metal Oxide Additives Incorporated Hydrogen Storage Systems: Formation of In Situ Catalysts and Mechanistic Understanding

D. Pukazhselvan, Narendar Nasani, S. K. Singh, and Duncan Paul Fagg

Contents

Abstract Hydrogen storage is a critical bottleneck to hydrogen economy. Presently none of the solid-state hydrogen storage materials (metal hydrides) reaches the capacity vs performance target (6.5 wt.% at 85 °C/5-12 bar, 1500 cycles) for the commercialization of light duty H_2 fuel cell vehicles. A few reversible hydrogen storage materials (e.g. MgH_2, $LiBH_4/MgH_2$ composite) possess adequate capacity, but their performance needs to be improved significantly. Metal oxide additives improve the hydrogen storage performance of metal hydrides, but the additive-hydride reaction mechanism remains not well understood. In this context, the present chapter discusses how various metal oxide additives interact with metal hydrides and

D. Pukazhselvan (✉) · D. P. Fagg
Nanoengineering Research Group, Department of Mechanical Engineering, University of Aveiro, Aveiro, Portugal
e-mail: dpuksel@gmail.com

N. Nasani
Centre for Materials for Electronics Technology, Pune, Maharashtra, India

S. K. Singh
Department of Physics, D.C.R. University of Science and Technology, Murthal, Haryana, India

R. Saravanan et al. (eds.), *Emerging Nanostructured Materials for Energy and Environmental Science*, Environmental Chemistry for a Sustainable World 23,
https://doi.org/10.1007/978-3-030-04474-9_5

facilitate the low temperature de/ab-sorption of hydrogen. The metal oxide additives may either directly catalyze the reaction without making any chemical changes or they catalyze indirectly by making active in situ products. In this chapter, various oxides and hydride combinations of the latter category are analyzed, and factors governing the improved hydrogen ab-/desorption performance are highlighted.

5.1 Introduction

Nanoparticles exhibit significantly improved electronic and surface chemical properties as compared to their bulk counterparts (Kelly et al. 2003; Sapra and Sarma 2004). Gold nanoparticles are the simplest example, for which size-dependent properties offer a wide diversity of potential applications, e.g., electronic circuits, sensors, probes, diagnostics, therapy, and catalysis (Daniel and Astruc 2004; Eustis and El-Sayed 2006; Haruta 2002). For a detailed explanation regarding the synthesis, characterization, and application of nanomaterials, the reader is directed to material-specific, in-depth studies reported in the literature (Bruce et al. 2008; Cao 2004; Chen and Mao 2007; Schwarz et al. 2004). In the present chapter, our interest is metal oxide nanoparticles, especially for catalytic applications. Since surface chemical features such as oxidation/reduction, gas ad-/ab-/desorption, complexation, and ion exchange properties determine the system performance, oxides are naturally the main choice as additives/catalysts and templates/supports in heterogeneous catalysis. There are various specific reasons why oxide surfaces are unique for catalytic applications: (i) the presence of cations and anions in a certain ratio that is relevant for influencing another species existing in chemical proximity, (ii) existence of bonding sites, (iii) existence of surface fields due to the coulombic nature of the ionic lattice, (iv) presence of charged adsorbed species, (v) presence of surface acidity or basicity, (vi) cationic/anionic vacancies, (vii) ability of cations to undergo oxidation/reduction reaction, (viii) ease of surface bridging with functional groups, (ix) high mobility of lattice oxygen and the possibility of oxygen-oxygen hopping, (x) creation of surface oxygen derived free radicals, etc. These properties are relevant for a wide variety of surface/bulk reactions, such as redox, oxidative Mannich reactions, condensation, deprotection, alkylation/hydroxylation, cycloaddition, dehydration, de-/re-hydrogenation, transesterification, organosynthesis, etc. Especially, in the case of metal-hydrogen interaction systems, when high-capacity metal hydrides exhibit thermodynamic and/or kinetic limitations, incorporation of suitable additives yield significantly improved hydrogenation/dehydrogenation performance (Zaluska et al. 2001; Zaluski et al. 1997).

A general universal classification of oxides is given in Fig. 5.1. Note that only transition metal oxides receive significant accolades for catalysis because the existence of partially filled d-shells of the metal ions and oxide ligands influences the neighboring atoms/molecules (Kung 1989). Usually binary/ternary metal oxides are routinely used in heterogeneous catalysis; however, mixed metal oxides, the oxygen-containing combinations of two or more metallic ions in a specific stoichiometry, are

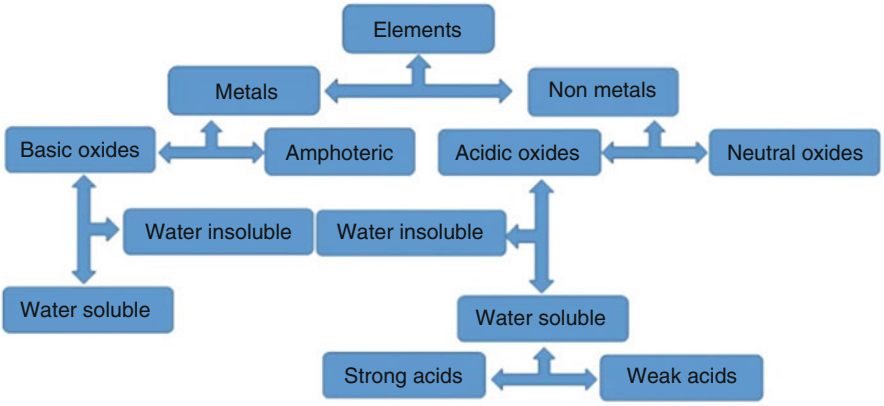

Fig. 5.1 Classification of oxides derived from the metals and non-metals

also useful additives under various circumstances (Gawande et al. 2012; Yuan et al. 2014). Especially for hydrogen storage systems, a wide variety of binary, ternary, and mixed metal oxides were employed as additives, and significant performance improvements have been reported. In the present chapter, we highlight how various metal oxides interact with the host hydride particles and mediate the reversible gas-solid surface interaction. The present chapter is organized as follows. Initially, by reciting the energy-wave vector/density of states (DOS) relationship for bulk, nano 3D, 2D, 1D, and 0D materials, the quantization effect implied by crystal dimension is highlighted. This section is followed by a brief summary to highlight a few classes of important metal oxides normally used for catalytic applications. Characteristics of oxide additives loaded hydrides belonging to few important categories, such as aluminates, binary hydrides, reactive hydride composites (RHC), and amide/imides, are reviewed. Catalysts existing without any structural/chemical changes throughout the reaction process are routinely reported in the literature. Therefore, in the present chapter, the main focus is on additives that undergo phase/chemical transformation to enhance the recycling performance of hydrogen storage systems. Some recent works performed by the authors in this line specifically on the promising hydrogen storage materials MgH_2 and $NaAlH_4$ are also highlighted in this respect.

5.2 Role of Size Effects

In heterogeneous catalysis, the size of the catalyst and the host particles are important factors influencing their interaction. Since sensitive electronic properties such as redox behavior/ionization and conductivity are strongly affected by domain size of the solid matter (particle/crystallite size) (Norris and Bawendi 1996; Zhang et al. 2009), for the understanding of readers, in the following, a brief explanation regarding the size-energy relationship is provided. A free electron existing in a

bulk 3D space (crystal structure) is free to move and no boundary conditions apply on the electron wave function. The energy-wave vector relation in this case is given by the relation,

$$E = \frac{\hbar^2 k^2}{2m} \tag{5.1}$$

As there are no restrictions, wave vector k is continuous and correspondingly energy values are continuous as shown in Fig. 5.2. On the other hand, when an electron is forced to confine in a 3D space, due to the potential barrier (V) existing at the boundaries of confined space "a," boundary conditions ("$\pm a$") apply. Therefore, the corresponding wave equation becomes solvable only for specific values of k and the derived value of k is given by the relation $k_n = n\frac{\pi}{a}$. Note that when "a" is high, the k_n values are small; hence the E vs k profile looks continuous. However, for the small values of "a," wave vector is bound to exhibit a substantial separation and since the wave vector is related with energy by a square function, the $E-k$ diagram shows an energy quantization effect. The corresponding $E-k$ diagram shown in Fig. 5.2 (top) is a simplest direct illustration that "confinement effect induces a circumstance called quantization." This quantization, how differs with a nanostructure where special restrictions exist in one or more directions, i.e., 2D, 1D, and quantum dots (OD), can be explained with the help of density of states (DOS) and energy relationships. For a 3D structure (nano), the density of states is given by the relation,

$$\mathrm{DOS}_{3\mathrm{D}} = \frac{8\pi\sqrt{2}}{\boldsymbol{h}^3} m^{\frac{3}{2}}\sqrt{E} \tag{5.2}$$

where m is mass of electrons ($9.109{*}10^{-31}$ kg), h is Planck's constant (6.626×10^{-34} J.s), $\hbar = h/2\pi$, and E is the energy accountable for the concerned states. Note that the $\mathrm{DOS}_{3\mathrm{D}}$ is directly proportional to the square root of energy as shown in the $\mathrm{DOS}_{3\mathrm{D}}$ vs energy profile of Fig. 5.2. In this case, although the electrons are confined than in the bulk material due to quantization, they have reasonable freedom to choose the states. On the other hand, when the structure is 2D, further confinement is forced due to the $\mathrm{DOS}_{2\mathrm{D}}$-energy relationship as shown by the expression:

$$\mathrm{DOS}_{2\mathrm{D}} = \frac{4\pi m}{\boldsymbol{h}^2} \tag{5.3}$$

In this case, the DOS is not proportional to energy (or proportional to E^0); hence, the DOS vs energy relation follows a step profile as shown in the figure. It means that only at specific energy values a significant number of states available for charge carriers when one degree of freedom is restricted. This situation, unlike the nano 3D case, forces electrons to occupy only certain states, ensuring higher confinement. When the movement of electrons is restricted in two directions, the $\mathrm{DOS}_{1\mathrm{D}}$ vs energy relation is given by,

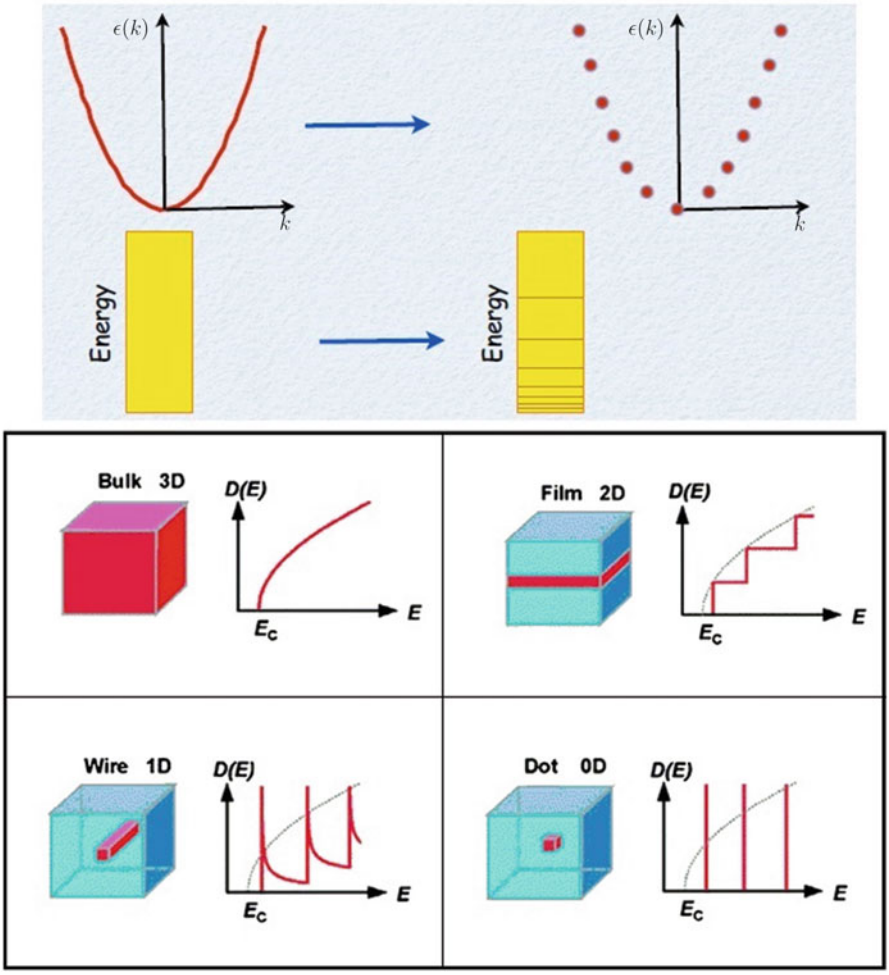

Fig. 5.2 Top: energy-wave vector diagram (*E-k* diagram) for a typical bulk and nano-3D structure. Bottom: density of states (DOS) vs energy profiles for dimension-controlled solid-state materials. (Adapted with permission from Handelman et al. 2012. Copyright © 2012, Royal Society of Chemistry)

$$\mathrm{DOS}_{1\mathrm{D}} = \frac{2\sqrt{2m^{\frac{1}{2}}}}{\sqrt{E}} \tag{5.4}$$

In this case the DOS is inversely proportional to the square root of energy, which implies a sharp decrease of states after a specific energy value. For the 0D materials, i.e., quantum dots, the $\mathrm{DOS}_{0\mathrm{D}}$ is a delta function as given in the following relation:

$$\mathrm{DOS}_{0\mathrm{D}} = 2\delta(E) \tag{5.5}$$

This relationship suggests that only with specific energy values, states can be accessed and everywhere except these is forbidden for electrons, ensuring high degree of confinement. The representation by Eqs. (5.1), (5.2), (5.3), (5.4) and (5.5), thus, provides a brief fundamental quantum mechanical explanation for readers regarding the origin of nanoconfinement. For a more detailed overview of mathematical expressions, the reader is directed to comprehensive quantum mechanical chapters discussed in the literature (Yu and Cardona 1996). In the case of metal oxides, apart from the naturally occurring size-dependent confinement effects (3D, 2D, 1D, or 0D structure), the surface chemical composition also significantly contributes to catalytic activity (Henrich and Cox 1996).

5.3 Metal Oxides for Catalytic Applications

Oxides commonly studied as catalysts/additives belong to the structural classes of corundum, rock salt, wurtzite, spinel, perovskite, rutile, and anatase structures. Table 5.1 summarizes these structure classes with a few examples. In fact there is no rule for the structural choice of oxides for catalytic applications. However, under certain circumstances, certain unique properties of a particular class of oxides look relevant for specific applications, and the catalyst is chosen accordingly.

Metal oxides are proven to be influential additives for almost every class of metal hydride systems. However, based upon the observations made for one hydride, the catalytic reaction mechanism cannot be generalized for every metal hydride systems. The oxide additive may be generated in situ or externally added, and the oxide may directly or indirectly catalyze the reaction. One interesting example for the in situ generated oxide additive that indirectly influences the metal-hydrogen interaction is lanthanum oxide existing in the $LaNi_5$ intermetallic/hydride system. The surface studies by spectroscopic methods clearly indicate a strong surface enrichment of oxidized La in $LaNi_5$ powder. When the intermetallic alloy $LaNi_5$ is exposed for a short time either in air or hydrogen gas (consisting oxygen impurities), oxidized La and Ni clusters are incorporated in the surface by the following reaction:

$$2\mathrm{LaNi}_5 + 1.5\,\mathrm{O}_2 \rightarrow \mathrm{La}_2\mathrm{O}_3 + 10\mathrm{Ni}. \tag{5.6}$$

A few authors have also identified the presence of $La(OH)_3$ and Ni clusters (Wallace et al. 1979). In either case, chemisorption of H_2 by Ni clusters was confirmed, as the studies identified a fermi surface at the top of the Ni 3D-derived states (Schlapbach 1981; Weaver et al. 1980). After breaking the H-H bond, the La oxide and Ni cluster interface act as a gateway for the diffusion of hydrogen inside the bulk $LaNi_5$. The same happens in the reverse direction during hydrogen release (Wallace et al. 1979). This is one of the simplest examples for in situ generated oxide

Table 5.1 Summary of common metal oxides used for catalytic applications (Categorized based upon crystal structure)

Crystal type	Lattice	Specific examples	Remarks
Corundum	Hexagonal	Al_2O_3, Ti_2O_3, V_2O_3, α-Fe_2O_3	General formula: M_2X_3
			Cations occupy distorted octahedral sites surrounded by six O legends
Rock salt	Face centered cubic	MgO, CaO, CoO, MnO, FeO, NiO	General formula: MX, where M at (0, 0, 0) and O at (1/2, 1/2, 1/2)
Wurtzite	Hexagonal	ZnO, β-$LiGaO_2$, β-$AgGaO_2$	General formula: MX
			Where M is at (1/3, 2/3, z) for z ~0.0 and is at (1/3, 2/3, z) for z ~0.38
Spinel	Cubic	$MgAl_2O_4$, Pb_3O_4 $CoFe_2O_4$, Na_2WO_4.	General formula: MM'_2X_4
			M and M′ are tetrahedrally and octahedrally coordinated cations
Perovskites	Simple cubic	$CaTiO_3$, BiF_2O_3, $BaZrO_3$, $LaAlO_3$	General formula: M′M″X
			M″ at cube corner positions (0, 0, 0), whereas M′ at (1/2, 1/2, 1/2) and O at face-centered positions (1/2, 1/2, 0)
Rutile	Tetragonal	TiO_2, V_2O_4, CrO_2, GeO_2, MoO_2, PbO_2	General formula MX_2 if the radius ratio r-/r+ exceeds ~1.37 MX2 favors rutile structure
			M at (0 0 0) and X at (x, x, 0) x~0.3
Anatase	Tetragonal	TiO_2, SnO_2	General formula MX_2
			M at (0 0 0) and X at (0 0 x) x~0.21

*Note: There is considerable confusion in the literature regarding the use of the word "catalysts" and "additives" for hydrogen storage systems. In general, catalysts take part in the chemical reaction but do not get consumed and hence not play any role in the thermodynamics of the system. Additives, on the other hand, may or may not get consumed in the reaction and may take part a role in the thermodynamics of the system. An additive may act as a catalyst, hence, when the role of the catalyst is not well understood, it is often safer to call it an additive

additives and their indirect effect on H sorption performance. In the case of high-capacity complex hydrides and binary hydrides, an external additive needs to be incorporated as hydrogen is strongly bonded with metal atoms. A large number of metal oxide additives and interesting materials aspects have been presented in the literature. In the following sections, we present a few metal oxide additives loaded hydrogen storage systems that are significant for commercial applications.

5.4 Metal Oxide Additives for High-Capacity Hydrogen Storage Systems

A few most important metal oxide additives studied in recent times is summarized in Table 5.2. When applying an oxide additive for improving the performance of a hydride, one may come across any of the following observations:

Table 5.2 Summary of a few most successful metal oxide additives studied for important high-capacity hydrogen storage systems

Hydride category	Specific example	Best oxide additives
Complex hydrides	$NaAlH_4$, $LiAlH_4$, $Mg(AlH_4)_2$	TiO_2, CeO_2, Nb_2O_5, $Ti(OBu)_4$
Binary hydrides	MgH_2, AlH_3	Nb_2O_5, r-GO, TiO_2, V_2O_5, Cr_2O_3, Fe_3O_4
Reactive hydride composites	MgH_2+2$LiBH_4$, $Ca(BH_4)_2$ + MgH_2	Sc_2O_3, Nb_2O_5, TiO_2/Ti_2O_3
Amide/imides	$LiNH_2$/2LiH, $Mg(NH_2)_2$/2LiH	K_2CO_3, K_3PO_4, $LiTi_2O_4$

(i) The additive remains chemically unchanged and provides consistently better system performance.
(ii) The additive reduces while mixing with hydride and improves the performance of the system.
(iii) The additive remains intact in the first cycle (or the first few cycles) but reduces during repeated cycles, improving the performance of the hydride.
(iv) The additive reduces during cycling runs but degrades the performance of the system.
(v) The additive gets reduced and makes new in situ catalysts, and the stable in situ catalyst improves the performance of the system for the long-term.
(vi) The additive makes a new in situ catalyst and provides better system performance, but the performance degrades due to slow compositional changes occurring to the catalyst. Whereas case (i) is straightforward, any of the situations (i)–(vi) can occur when an oxide additive is incorporated with a hydride.

In experimental context, our requirement is to obtain higher system performance, no matter whatever mechanistic category, among (i)–(vi), the additive/catalyst undertakes.

5.4.1 Metal Oxides Loaded Aluminates

Owing to the good H/M ratio, lightweight aluminates ($MAlH_4$ and $M'(AlH_4)_2$, M = Li, Na, K and M′ = Ca, Mg) receive considerable interest for hydrogen storage applications (Orimo et al. 2007). Among all the aluminates, good reversibility is reported only for two aluminates, $NaAlH_4$ and $KAlH_4$ (Bogdanović and Sandrock 2011; Morioka et al. 2003; Pukazhselvan et al. 2012, 2015), and their working temperature range is identified to be 180–350 °C. By incorporating additives, better performance can be achieved, but the mechanism of hydrogen release/reabsorption is not well understood (Bogdanović et al. 2007). In order to successfully tailor new promising reversible complex hydrides, it is necessary to understand the exact mechanism of H de-/absorption promoted by additives. Since sodium alanate ($NaAlH_4$) is the best model system in the category of aluminates, for mechanistic

studies, researchers prefer $NaAlH_4$ over other aluminates (later on the acquired knowledge can be extended to other aluminates). Since aluminum contains only three valence electrons for covalent bonding with hydrogen, the stable existence of Al-H covalently bonded $[AlH_4]^-$ tetrahedral complex relies on its ionic bond strength with Na^+ ion. The catalyst/additive should stimulate the antibonding between Na^+ and $[AlH_4]^-$ ions for the liberation of hydrogen atoms. The circumstance of the additive/catalyst may correspond to any of the cases (i)–(vi) mentioned above (Sect. 5.4), but antibonding will be stimulated only when the additive/catalyst possesses appropriate electronic features for depleting the stabilizing electron from the complex $[AlH_4]^-$. It is interesting that, in the literature, additives falling across all the categories (i)–(vi) have been reported for $NaAlH_4$/$LiAlH_4$. A few of them are discussed below.

Lee et al. (2007b) performed a comparative study for 10 wt.% lanthanide oxides, La_2O_3, CeO_2, Sm_2O_3, and Gd_2O_3 mixed $NaAlH_4$ and suggested that all these oxides trigger higher kinetics at lower dehydrogenation temperatures as compared to neat $NaAlH_4$. XRD investigation suggested that except CeO_2 additive which transforms to cerium hydride, all other oxides remain unchanged. Among these oxides, Sm_2O_3 additive was found to be the best for improving the reaction kinetics, reversibility, and cyclic stability. Xuanhui et al. (Rafi ud et al. 2012) used Nb_2O_5, TiO_2, and Cr_2O_3 nanoparticle additives for $NaAlH_4$ and found that TiO_2 and Nb_2O_5 are better than Cr_2O_3. The authors observed the reduction of TiO_2 and Nb_2O_5 in the first cycle itself. Xuanhui et al. (Rafi ud et al. 2011) also tested the dehydrogenation behavior of Nb_2O_5 and Cr_2O_3 additives loaded $LiAlH_4$ and found that both additives improve the desorption of hydrogen at lower temperatures as compared to additive-free samples but Nb_2O_5 is the best among these additives. After ball milling with $LiAlH_4$ for 30 min, both Nb_2O_5 and Cr_2O_3 additives remain chemically unchanged. However, the powder tested after dehydrogenation measurements suggests that whereas Cr_2O_3 remains chemically unchanged Nb_2O_5 additive reduces during the first cycle dehydrogenation. Apparently, the existence of three different Nb variants, NbO_2, NbH, and $LiNbO_3$, was identified, but it is not exactly clear which product among these was responsible for catalytic activity. Notwithstanding, the authors suggested that the variable valence states of Nb incorporated in the powder may be a prime reason for the catalytic activity. Although such a claim requires further verification, it is interesting that the reduction of additive and the subsequent formation of multiple in situ additive(s) helps to destabilize the complex hydride. In another study, Li et al. (2013) used $NiFe_2O_4$ additive for $LiAlH_4$ and found that the additive interacts with $LiAlH_4$ during ball milling itself and forms $LiFeO_2$ and Al-Ni alloy (Al_4Ni_3). During dehydrogenation, these in situ products further interact chemically and produce $LiAlO_2$ and $Al_{1.1}Ni_{0.9}$ products. The authors suggested that the synergetic effect of these products is the reason behind the superior performance of the system.

In one of the authors' earlier studies (Pukazhselvan et al. 2010), the hydrogen storage behavior of metal oxide nanoparticle additives such as TiO_2, CeO_2, La_2O_3, Pr_2O_3, Nd_2O_3, Sm_2O_3, Eu_2O_3, and Gd_2O_3 loaded $NaAlH_4$ was tested, and it was found that TiO_2 is the most effective additive. This observation is in agreement with the findings of Lee et al. (2008) who used 2 mol.% TiO_2 nanopowder for catalyzing

$NaAlH_4$. The thermodynamic calculations of Lee et al. further revealed that titania reacts with $NaAlH_4$ to form an intermetallic phase $TiAl_3$ in the mixture. Usually pure $NaAlH_4$ releases 5.5 wt.% hydrogen through a two-step decomposition reaction, first step at 180 °C and second step at 230 °C, as given by the reaction (5.7):

$$3NaAlH_4 \leftrightarrow Na_3AlH_6 + 2Al + 3H_2 \leftrightarrow 3NaH + 3Al + 4.5H_2. \quad (5.7)$$

As per the thermodynamic calculations of Lee et al., 2 mol.% TiO_2 reacts with $NaAlH_4$ by the following reaction:

$$0.98NaAlH_4 + 0.02TiO_2 \rightarrow 0.859NaAlH_4 + 0.073Na_3AlH_6 + 0.011Al_2O_3 + 0.013TiAl_3 + 0.044H_2 \quad (5.8)$$

The 1.3 mol.% $TiAl_3$ derived from 2 mol.% TiO_2 catalyzes the remaining 85.9 mol.% $NaAlH_4$ and 7.3 mol.% Na_3AlH_6 and lowers the H desorption temperature by at least 30–50 °C while also appreciably increasing the reaction kinetics. The existence of 1.1 mol.% alumina is believed to have no impact as alumina is not a fine catalyst for $NaAlH_4$ (Ma et al. 2012). Another study that directly employs mechanochemically synthesized $TiAl_3$ as catalyst proves that $TiAl_3$ exhibits a pronounced catalytic activity for $NaAlH_4$ (Lee et al. 2007a). It may herewith be recalled that the well-studied $TiCl_3$ additive also makes $TiAl_3$ by the following reaction:

$$0.98NaAlH_4 + 0.02TiCl_3 \rightarrow 0.916NaAlH_4 + 0.025Na_3AlH_6 + 0.010NaCl + 0.013TiAl_3 + 0.036H_2 \quad (5.9)$$

Various forms of Ti-based additives, Ti nanoparticles (Fichtner et al. 2003), chlorides/fluorides (Majzoub and Gross 2003), and oxides/alkoxides (Bogdanović et al. 2003; Pukazhselvan 2012), were tried for $NaAlH_4$, and formation of in situ Ti_xAl_y intermetallic alloy was identified for many of these cases. The chemical state of reduced titanium and its coordination in the Ti_xAl_y alloy were well studied by various researchers (Bogdanović et al. 2007; Léon et al. 2004), and it is concluded that Ti exists in zerovalent state that does not change by hydrogenation/dehydrogenation cycles. Felderhoff et al. (2004) identified slight structural changes for Ti_xAl_y alloy during charging/discharging cycles, but the zero valence of Ti is always maintained. Following these observations, Pukazh et al. tested a 10 mol.% TiO_2 loaded $NaAlH_4$ powder and explored further details regarding the reduction of titania and the Ti_xAl_y in situ additive (Pukazhselvan 2012). The results are demonstrated by XRD as shown in Fig. 5.3.

The existence of anatase titania peak in profile “a” of Fig. 5.3 suggests that although a partial reduction may be possible during mechanical milling, a major portion of the titania additive remains unreacted. Profile “b” suggests that reduction of TiO_2 takes place during the first de-/re-hydrogenation cycle, but a smaller part still

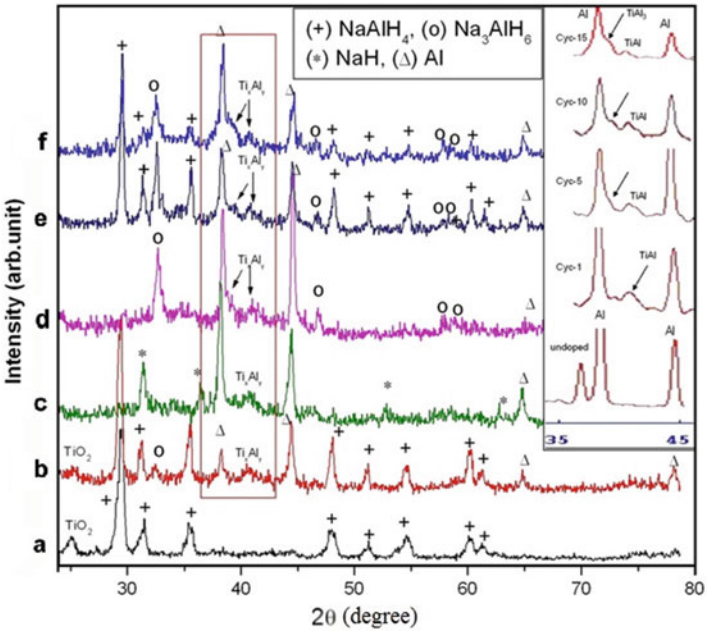

Fig. 5.3 XRD profiles of 10 wt.% titania additive mixed $NaAlH_4$ tested for various cycles. (**a**) 10 mol% TiO_2 (25 nm):$NaAlH_4$ ball milled (1 h) starting material. (**b**) Re-hydrogenated powder of the 1st cycle dehydrogenated material, (**c**) 2nd cycle dehydrogenated powder, (**d**) 6th cycle dehydrogenated (to 1st step), (**e**) 10th cycle hydrogenated, and (**f**) 15th cycle hydrogenated. (Reproduced with permission from Pukazhselvan 2012, Copyright © 2012 Hydrogen Energy Publications. Elsevier.

Note* The existence of Ti_xAl_y alloy in the Ti/Ti variant additives loaded $NaAlH_4$ powder was a chapter of intense debate in the literature. In the early days of research, its presence could not be confirmed due to two reasons: (i) The size of Ti_xAl_y crystallites is too small; hence when a small concentration of additive is used, its XRD peaks get hindered by the background noise (in some cases amorphous Ti_xAl_y is also reported). (ii) The peak position of Ti_xAl_y alloy is closer to the peak position of Al(111) peak; hence it is discernible only as a shoulder to the Al (111) peak (in the Ti_xAl_y alloy family, several alloy combinations show XRD reflections in the range 39–44° 2θ, and among these $TiAl_3$ is a widely known alloy whose peak position is too close to Al(111) for simple deconvolution. Using higher additive concentrations is therefore recommended for characterization studies; however, for hydrogen storage studies, the additive concentration should be as little as possible)

remains unreacted at the end of first cycle. The XRD profiles corresponding to cycles 2 and 6 (profiles "c" and "d," respectively) show no presence of TiO_2. It is clear from these results that titania reduces completely during the second cycle and the reduced Ti combines with Al (Ti_xAl_y phase peak position, 40.8°). Upon cycling the sample further, as revealed by comparing profiles "d," "e," and "f," the formation of another phase of Ti_xAl_y alloy (Schoenitz et al. 2004) is also identified (position 39.9°, right-side shoulder to Al(111) peak. For clarity, this is highlighted in the inset). This observation possibly indicates the transformation of one Ti_xAl_y phase to another

during repeated H ab-/desorption cycles. Further studies may provide more clarity for these observations. However, these observations are enough to conclude that in certain cases, metal oxides get reduced and make new in situ products, and the in situ product itself get chemically and/or structurally modified upon catalyzing the reaction. It is therefore a challenge for material scientists to identify the most promising composition for most active catalytic performance and retain the optimum catalyst concentration/structure during cyclic studies. Presently although the actual chemical species (Ti_xAl_y) responsible for catalytic activity is confirmed, further studies are required to know how it influences the ionic $Na^+ - [AlH_4]^-$ and covalent Al-H bonds. Extensive theoretical studies for understanding the electronic structure of Ti_xAl_y will throw further light on the bond breaking/making mechanism of $NaAlH_4$.

5.4.2 Metal Oxides Loaded Magnesium Hydride

The high capacity reversible binary hydride, MgH_2 (7.6 wt.% and 110 g/L), is another potential solid-state system for hydrogen storage. However, owing to the high enthalpy of formation ($\Delta H = -76$ kJ/mol), MgH_2 requires temperature over 300 °C for the release of hydrogen at 1 bar equilibrium pressure (Pukazhselvan et al. 2012). Extensive research works have, thus, been conducted for enhancing the hydrogen storage performance of MgH_2 through various strategies (Kalidindi and Jagirdar 2009; Pukazhselvan et al. 2014b; Zhao-Karger et al. 2010; Zlotea et al. 2015), e.g., (i) size tailoring, (ii) nanoconfinement, (iii) chemical modification, (iv) additive loading, etc. Nevertheless, considering the context of the present chapter, we restrict our discussion to category "iv," especially on metal oxide additives. Various metal oxides, transition metal oxides (Jung et al. 2006), rare earth oxides (Sadhasivam et al. 2013), mixed ternary oxide phases (Patah et al. 2009; Rahman et al. 2011), and rock salt oxides (Pukazhselvan et al. 2014a) were used by researchers for improving the dehydrogenation of MgH_2. It is widely agreed that metal oxide additives are the best for MgH_2, but the catalytic reaction mechanism of metal oxides added MgH_2 remains a chapter of intense debate. In this context, by referring some significant results reported in the literature, we attempt to provide a reasonable understanding regarding the mechanistic role of best metal oxide additives for MgH_2.

The formation enthalpy of MgO, −601 kJ/mol, is a much higher value than the formation enthalpy of MgH_2, i.e., −76 kJ/mol. Therefore, naturally the tendency of Mg oxidation is higher when the system contains oxygen impurities. Formation of MgO as a result of oxidation of Mg in the surface of Mg/MgH_2 is believed to be a serious contamination effect that impedes the Mg-H sorption interaction. Therefore, the additive/catalytic selectivity steers two considerations: (i) additives that incorporate surface oxide contaminants need to be avoided, and (ii) additives that offer clean surface and facilitating Mg-H interaction need to be deployed. In order to protect the Mg/MgH_2 surface from oxygen/moisture, some methods have been suggested in the literature, such as embedding MgH_2 on gas-selective polymers (e.g., PMMA) or encapsulating with graphene or graphene oxide layers. These

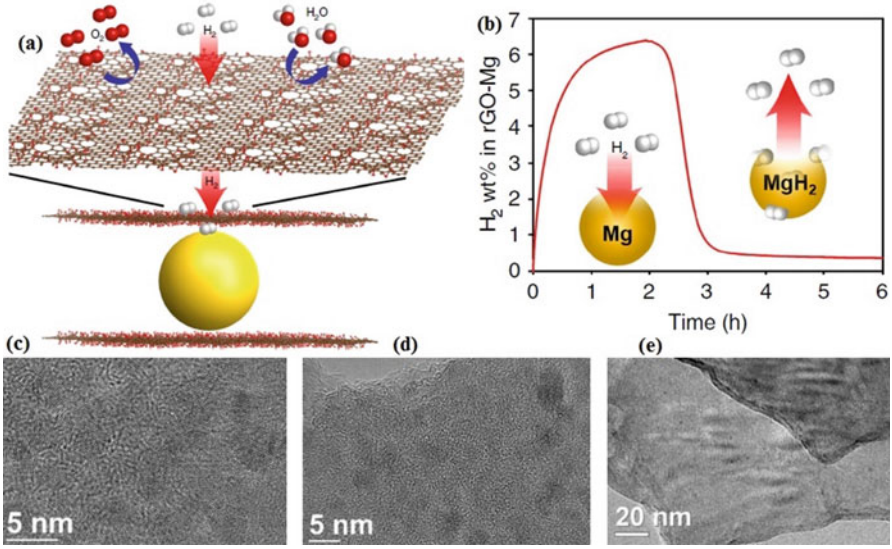

Fig. 5.4 (**a**) Pictorial representation of Mg laminated by rGO, (**b**) hydrogen ab-/desorption kinetics profile of Mg crystals laminated by rGO sheets, (**c**) HRTEM image of as-prepared Mg-rGO laminates, (**d**) HRTEM image of Mg-rGO laminates after hydrogenation, and (**e**) overview of one portion of the rGO-laminated MgH_2 sample. (Reproduced from the work of Cho et al. 2016 Copyright © 2016, Springer Nature)

surface protectors prevent the intrusion of larger molecules, such as O_2, N_2, and H_2O, while facilitating the permeation of hydrogen (Jeon et al. 2011; Kim et al. 2013). Recently Cho et al. (2016) have demonstrated a method to laminate Mg nanoparticles by using reduced graphene oxide (rGO) and suggested that it is a good method for preventing surface oxidation. As shown in the pictorial representation (Fig. 5.4a), Cho et al. showed that about 3.3 nm sized Mg nanocrystals can be laminated by large sheets of rGO by complexing GO with bis(cyclopentadienyl) magnesium and then reducing it by treating with lithium naphthalenide solution. As shown in Fig. 5.4b, the rGO-laminated Mg instantly absorbs (200 °C/15 bar H_2 pressure) over 6 wt.% H_2 and desorbs all hydrogen (300 °C/vacuum). Moreover, the results are consistent even after 3 months of exposure in air. The HRTEM images shown in Fig. 5.4c and d, respectively, correspond to rGO-laminated Mg and its hydrogenated counterpart. Figure 5.4e represents the overview of one portion of the rGO-laminated MgH_2 sample. The data shown in Fig. 5.4 clearly reveals that Mg/MgH_2 nanoparticles are well confined and stable over the conditions applied for recycling tests. Based upon DFT studies and Mg K-edge X-ray absorption spectra, Wan et al. (2017) have recently explored that when MgO nanoparticles are sealed by rGO, the outermost atomic layer of Mg gets slightly oxidized and forms a monolayer honeycomb MgO. Whereas the bulk MgO rock salt is known as a potential H diffusion barrier, the monolayer MgO formed as a result of interaction with rGO provides no barrier and in fact works similarly to a clean Mg surface. It is

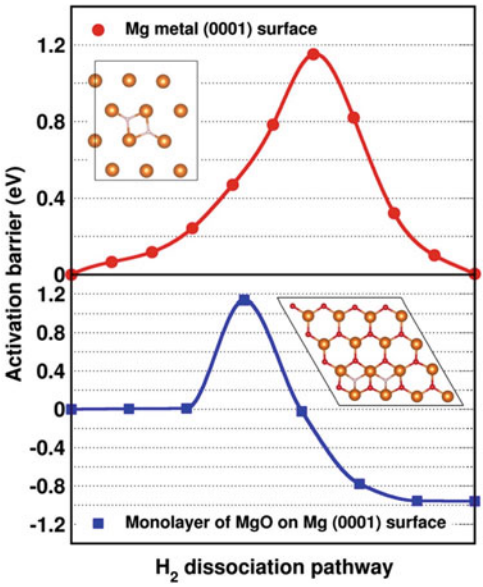

Fig. 5.5 Hydrogen molecular dissociation energy profile for clean Mg surface and monolayer MgO covered Mg surface. (Reproduced with permission from Wan et al. 2017. Copyright © 2017, American Chemical Society)

also in agreement with the work of Kobayashi et al. (Kobayashi et al. 1994) that suggested that thin MgO substrates exhibit suitable electronic structure for the chemisorption of hydrogen molecules.

By applying density functional theory, Wan et al. calculated the H_2 dissociation energy profile for clean Mg surfaces and monolayer MgO covered Mg surfaces as demonstrated in Fig. 5.5. As seen, the H_2 dissociation energy is the same value (1.14 eV) for both surfaces. Nonetheless, once the H-H bond is broken, the MgO-layered system relaxes to a much lower energy state, roughly about 1 eV lower than the initial H_2 physisorbed state at a distance of 2.9 Å away from the surface. Note that when a few layers of such honeycomb structured MgO deposits over another, it results to the formation of a bulk rock salt MgO structure, which is well known as hydrogen diffusion barrier. Hence, from the understanding gained from this study, a valid question arises that whether the proven best oxide additives play a role to restrict the growth of the MgO and lead to a circumstance as presented in Fig. 5.5. Moreover, there are also convincing data that supports (Wu et al.) that the energy required to break the dihydrogen bond on the MgO surface varies depending on the sites where H_2 faces the MgO surface (Wu et al. 2009). In another work, Borgschulte et al. (2008) investigated the surface composition and chemical state of ball-milled MgH_2 by XPS and H/D exchange experiments. This study confirms the existence of MgO wrapped surfaces with cationic vacancies having catalytic tendencies. These studies give us two interesting pieces of information: (i) not all the MgO surfaces are inactive for Mg-H interaction, and (b) tuning the chemistry of the MgO surface may be a critical step in the process of catalysis for reducible metal oxide additives loaded MgH_2 system.

Proceeding with the above information, in the following, we reviewed a few important results reported for various metal oxide additives loaded MgH_2. In some of these studies, the existence of oxidized Mg surfaces was proven, but the catalytic contribution of this oxidized Mg surface was considered insignificant. Hanada et al. (2009) used 1 mol % of transition metal oxide nanoparticle additives such as Nb_2O_5, V_2O_5, and TiO_2 and showed that all these products after dehydrogenation show the coexistence of Mg and MgO without any traces of intact additives. The K-edge XANES spectra revealed the existence of the used additives in partially reduced state. Based upon these observations, the authors concluded that improved hydrogen sorption is due to the formation of reduced oxides. However, in this study it was not detailed how influential was the existence of an oxidized Mg surface. Oelerich et al. (2001b) investigated the hydrogen absorption/desorption behavior of MgH_2 by incorporating a range of metal oxide additives, such as Sc_2O_3, TiO_2, V_2O_5, Cr_2O_3, Mn_2O_3, Fe_3O_4, CuO, Al_2O_3, and SiO_2. By this comparative study, the authors categorized the additives from most effective to the least effective. For example, for hydrogen absorption, a nearly similar effect was observed for TiO_2, V_2O_5, Cr_2O_3, Mn_2O_3, Fe_3O_4, and CuO additives. On the other hand, for dehydrogenation, Fe_3O_4 and V_2O_5 show comparable effects, followed by Mn_2O_3, Cr_2O_3, and TiO_2 additives. It was shown that only 0.2 mol.% of the additive is sufficient for providing fast sorption kinetics. However, details regarding why certain oxides are better than others for MgH_2 were not explored.

Oelerich et al. (2001a) made a comparative hydrogen storage test for MgH_2 using various forms of vanadium additives, such as V, V_2O_5, VN, and VC. This study confirms that vanadium oxide is better than other forms of vanadium additives. Further studies revealed that V_2O_5 gets reduced during processing the powder toward H ab-/desorption measurements. Porcu et al. (2008) observed that the Nb_2O_5 additive reacts with MgH_2 and oxidizes a significant portion of MgH_2. Polanski et al. (Polanski and Bystrzycki 2009) performed comparative hydrogen storage measurements for Cr_2O_3, TiO_2, Fe_3O_4, Fe_2O_3, In_2O_3, and ZnO additives mixed MgH_2 and suggested that Cr_2O_3, TiO_2, Fe_3O_4, and Fe_2O_3 additives are better than indium and zinc oxides for improving the dehydrogenation of MgH_2. Later on, Polanski et al. (2011) used Cr_2O_3 nanoparticle additive for MgH_2, and an ab-/desorption study for 150 cycles revealed that reduction of Cr_2O_3 leads to the formation of Cr and MgO. A substantial capacity reduction was observed due to the loss of Mg as MgO and the consequent microstructural changes. Patah et al. (2009) observed that co-catalyzing MgH_2 by Nb_2O_5 and Cr_2O_3 provides better effect than when these additives were incorporated separately. The authors suggested the generation of diffusion paths as the reason for the result; however, no further information was added how the diffusion pathways are generated by mixing together the Nb_2O_5 and Cr_2O_3 additives. Croston et al. (2010) used titania additive for improving the dehydrogenation of MgH_2 and suggested that titania is reduced by its interaction with MgH_2. Huang et al. (2006) used oxides of iron, such as Fe_2O_3 and Fe_3O_4 as additives for MgH_2 and found that during heating, both iron oxides reduce to pure Fe. For both samples, there were no substantial differences in catalytic activity in terms of decreasing the desorption temperature and increasing the reaction

kinetics. However, a slightly higher loss of capacity for Fe_2O_3 additive loaded sample as compared to Fe_3O_4 additive loaded sample was observed. The authors suggested the capacity, especially for $MgH_2 + Fe_2O_3$ composite, to be a result of the reduction reaction, as more magnesium is lost to MgO in this mixture. In these studies, the role of MgO is ignored, at times referring this as an unintended reaction product and a potential barrier layer incorporated in the system by consuming useful magnesium. Friedrichs et al. (2006c) observed that the Mg/MgH_2 samples exhibit a strong tendency for surface oxidation and an oxide passivation layer, size 3–4 nm, forms instantly in MgH_2/Mg samples upon the availability of oxygen impurities. This study further revealed that once the surface is neatly covered by a thin layer of MgO, further oxidation does not occur. These studies necessitate an in-depth study for exploring the details of oxide-MgH_2 chemical interaction and its role on the catalysis of the system. The information observed through these studies suggest that the MgO layer existing in oxide additives loaded MgH_2 cannot be ignored as a barrier layer as was thought previously.

Among all the metal oxide additives reported in the literature, Nb_2O_5 is the most widely investigated additive for MgH_2. Barkhordarian et al. (2003) revealed that Nb_2O_5 additive loaded MgH_2 at the reaction temperature of 300 °C releases about 7 wt.% hydrogen within 130 s and reabsorbs it within 60 s. Friedrichs et al. (2006a) used 15 nm- and 100 nm-sized Nb_2O_5 additives for MgH_2 and observed that, whereas both sizes are beneficial, smaller particles strongly enhance the kinetics of the reaction. In another study Hanada et al. (2005) showed that in the case of a 1 mol. % Nb_2O_5 admixed material, the required dehydrogenation temperature is reduced by at least 50 °C in the second cycle as compared to the first cycle. Note that the performance improvement during cycling measurements is a sign for the formation of modified in situ additives. Although all these results are in good agreement with each other, regarding mechanistic understanding, considerable anomalies exist in the literature. Aguey-Zinsou et al. (2007) suggested that Nb_2O_5 acts as lubricant, dispersing and/or cracking agent during milling and helping to further reduce MgH_2 particle size, while no chemical changes occur to Nb_2O_5 during cyclic measurements. Further exemplary studies, however, revealed that Nb_2O_5 in fact gets reduced chemically and a significant amount of oxidized Mg gets incorporated in the powder.

Presently it is clear that some of the best metal oxide additives reported for MgH_2, for example, Nb_2O_5 and TiO_2, involve a chemical interaction with MgH_2 to make active in situ catalysts. However, there are contradictory opinions in the literature regarding the exact chemical composition of the reduced in situ catalyst. Ma et al. reported that Nb nanocrystals of size ~10 to 20 nm are the apparent reaction product when ball milling MgH_2/Nb_2O_5 mixture and these nanocrystals may be responsible for the catalytic activity (Ma et al. 2013). Friedrichs et al. (2006a) suggested the formation of oxygen deficient magnesium niobate ($MgNb_2O_{3.67}$) in the Nb_2O_5 added MgH_2 samples. However, their further study suggested the composition to be $Mg_xNb_{0.8(1-x)}O$ (Friedrichs et al. 2007). By an in situ X-ray diffraction study, Nielsen and Jensen identified that Nb dissolved MgO forms during the dehydrogenation of Nb_2O_5 additive loaded MgH_2 (Nielsen and Jensen 2012). Recently Pukazh

et al. employed Nb_2O_5 and TiO_2 additives for MgH_2 and showed that metals substituted MgO rock salt products, typified by $Mg_xNb_yO_{x+y}$/$Mg_xTi_yO_{x+y}$ form as a result of chemical interaction between the additives with MgH_2, and this rock salt is responsible for the catalytic activity (Pukazhselvan et al. 2016a, 2017a). Recent theoretical calculations of Sandhya et al. by DFT modeling also support these observations (Pukazhselvan et al. 2017b; Sandhya et al. 2016).

Pukazh et al. made composite mixtures of MgH_2+nNb_2O_5 (n = 0.083, 0.10, 0.123, 0.167, 0.25, 0.50, 1.0, and 1.5) and tested the mechanochemical reaction products for three sets of reaction times, such as 1 h, 10 h, and 30 h (totally 24 samples) (Pukazhselvan et al. 2016a). The best composition out of these 24 samples, i.e., MgH_2+0.167Nb_2O_5, was then studied by varying the reaction time, i.e., 2 min, 5 min, 15 min, 30 min, 45 min, 1 h, 2 h, 5 h, 10 h, 15 h, 20 h, 25 h, and 30 h (Pukazhselvan et al. 2016d). The corresponding XRD profiles of these samples are shown in Fig. 5.6. As seen at the initial stage (15 min to 5 h) of mechanochemical

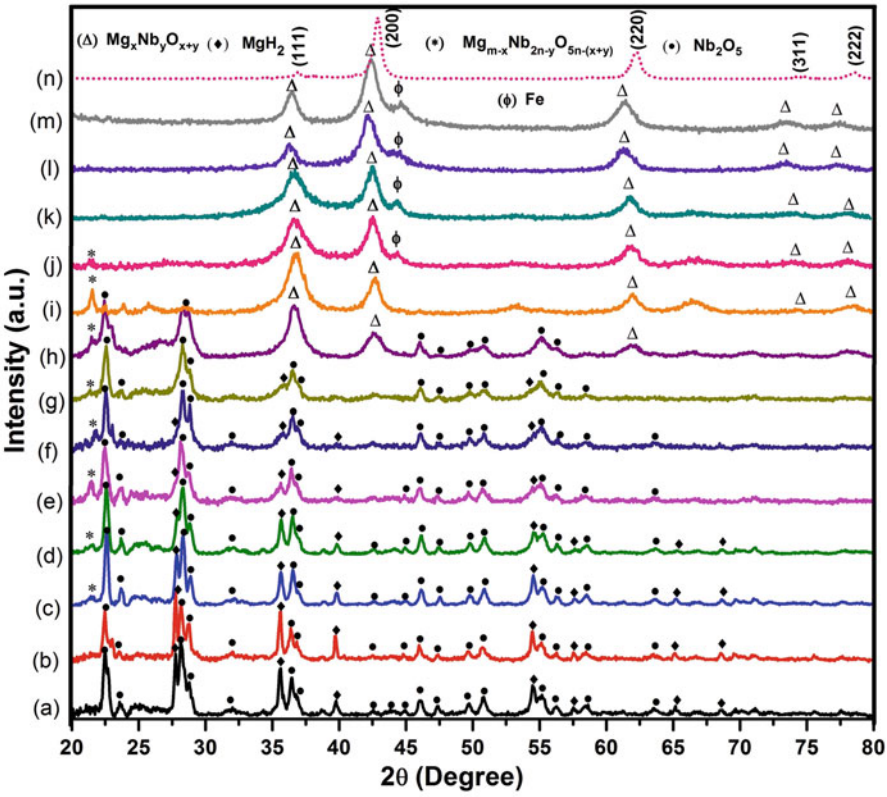

Fig. 5.6 Mechanochemically reacted MgH_2+0.167Nb_2O_5 powder for (**a**) 2 min, (**b**) 5 min, (**c**) 15 min, (**d**) 30 min, (**e**) 45 min, (**f**) 1 h, (**g**) 2 h, (**h**) 5 h, (**i**) 10 h, (**j**) 15 h, (**k**) 20 h, (**l**) 25 h, and (**m**) 30 h and (**n**) standard MgO rock salt. (Reproduced with permission from Pukazhselvan et al. 2016d, Copyright © 2015, John Wiley and Sons)

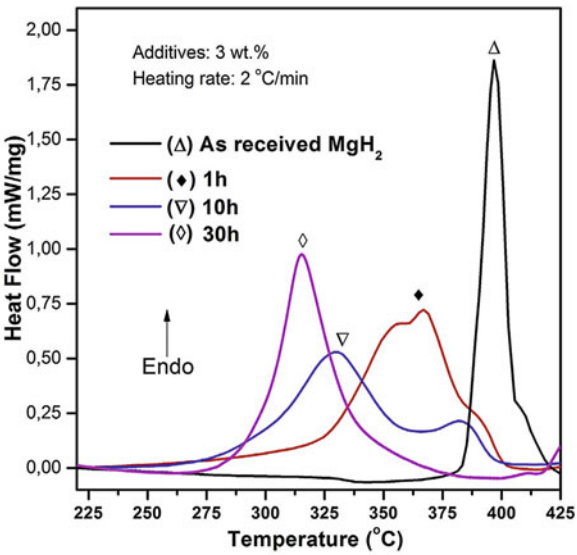

Fig. 5.7 DSC profiles of MgH_2 added with a 3 wt.% of 1h, 10h and 30h reacted additive (MgH_2+0.167Nb_2O_5). Symbols: (▯) as-received MgH_2; (◆)1 h reacted additive powder mixed with MgH_2; (▿)10 h reacted additive powder mixed with MgH_2; (◊)30 h reacted additive powder mixed with MgH_2. (Reproduced with permission from Pukazhselvan et al. 2016a. Copyright © 2015 Hydrogen Energy Publications, LLC. Elsevier)

reaction, MgH_2 disappears gradually, and an unidentified phase (indexed by * symbol) forms in minor quantities. During 5–15 h of reaction, dominant existence of a monophase rock salt product with characteristic (111), (200), and (220) reflections can be noticed. Upon further increasing the milling time up to 30 h, a monophase with visibly unchanged XRD features after 25 h, having close crystallographic resemblance with MgO rock salt is observed. Further spectroscopic/microscopic studies suggested that the product existing in 30 h reacted material is actually Nb incorporated MgO, typified by a general formula, $Mg_xNb_yO_{x+y}$. Samples taken from 1 h, 10h, and 30h reacted powders were used as additives (3 wt.%) for MgH_2, and the DSC profiles were recorded. The DSC profiles demonstrated by Fig. 5.7 show a systematic shift toward lower temperatures with a series, 30 h > 10 h > 1 h > no additive. This result shows that the rock salt product $Mg_xNb_yO_{x+y}$ possesses a significant catalytic behavior for the low-temperature dehydrogenation of MgH_2. Following this study, Pukazh et al. explored a similar observation for titania added MgH_2 through an XRD/in situ XRD study performed for a 10 wt.% titania loaded MgH_2 (Pukazhselvan et al. 2017a). As it can be seen in the in situ XRD shown in Fig. 5.8, reduction of titania resulting to evolution of a new phase closer to the peak position of MgO can be observed (compare the MgO peak position from Fig. 5.6) upon increasing the temperature. Further characterization studies by XRD, HRTEM, and elemental chemical mapping techniques revealed the existence of homogeneously distributed Ti in a crystalline rock salt matrix ($Mg_xTi_yO_{x+y}$) which is similar to that observed for the Nb_2O_5 loaded MgH_2 system. Note that MgO and metals dissolved MgO (e.g., $Mg_xTi_yO_{x+y}$/ $Mg_xNb_yO_{x+y}$) exhibit almost identical crystallographic features; hence its existence is usually overlooked by many researchers. Sandhya et al. (2016) recently revealed that incorporation of Nb in the Mg site of

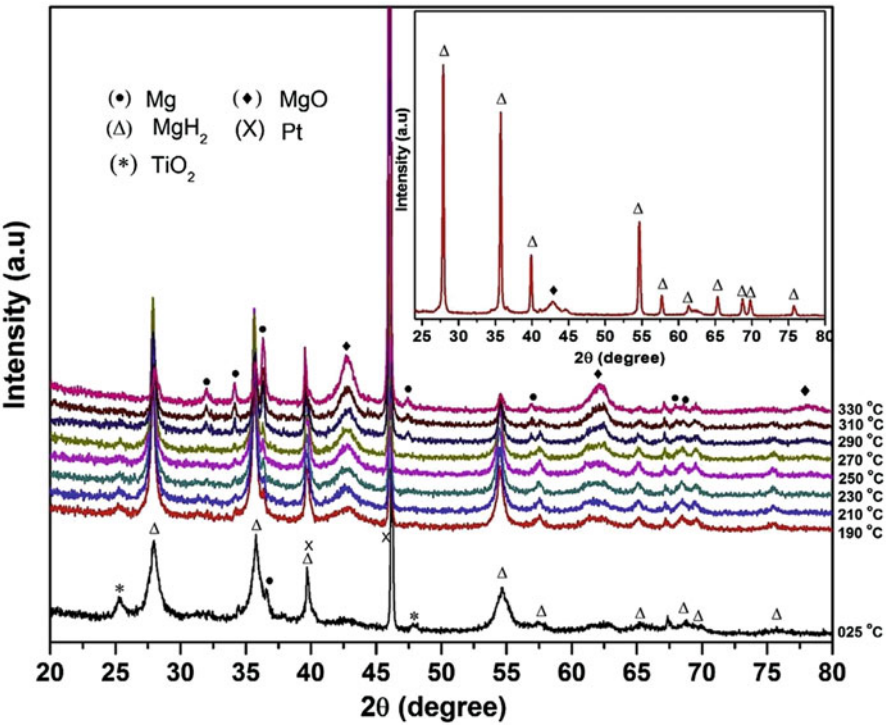

Fig. 5.8 In situ XRD patterns of 10 wt.% TiO_2 added MgH_2 (5 h milling). Inset shows the XRD of the re-hydrogenated sample. (Reproduced with permission from Pukazhselvan et al. 2017a, Copyright © 2017 Elsevier)

MgO rock salt structure results in an improved electronic behavior and hence is very active for catalytic interaction with MgH_2 and H_2.

From these understandings, a surface reaction model shown in Fig. 5.9 (Pukazhselvan et al. 2016c) seems to be a logically valid model for Nb_2O_5 loaded MgH_2. As shown in Fig. 5.9a, the commercial Mg/MgH_2 samples usually contain thin MgO rock salt layers in the surface. When the surface MgO rock salt layer is thick as shown in Fig. 5.9b, the system requires high operating conditions because of the high diffusion barrier caused by MgO. On the other hand, when Nb replaces few Mg spots (i.e., $Mg_xNb_yO_{x+y}$), the rock salt layer becomes catalytically active because of modifications in its electronic structure. Earlier in Fig. 5.6, it was shown that $Mg_xNb_yO_{x+y}$ forms from the reaction between MgH_2 and Nb_2O_5 additive. Hence the MgH_2 particles sealed by $Mg_xNb_yO_{x+y}$ shells as shown in Fig. 5.9c seems to be apparently a valid model for Nb_2O_5 loaded MgH_2. Note that the insertion of Nb, having a slightly higher ionic size than Mg, may also make fractures in the rock salt lattice. Moreover, since XPS study (Pukazhselvan et al. 2016b) proves the existence of a small amount of Nb-O secondary phase(s) other than $Mg_xNb_yO_{x+y}$, the presence of $NbO_x/Mg_xNb_yO_{x+y}/Nb$ interface cannot be

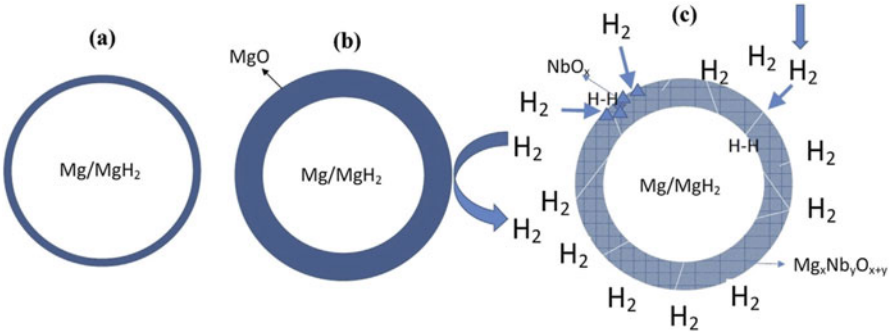

Fig. 5.9 Schematic representation for enhanced diffusion of hydrogen across the MgO shells, (**a**) thin MgO shell in commercial MgH_2 samples, (**b**) surface passivated Mg/MgH_2 particles due to thick MgO shells, and (**c**) active Nb dissolved MgO surface/interface layer. (Reproduced with permission from Pukazhselvan et al. 2016c. Copyright © 2016 Hydrogen Energy Publications. Elsevier)

ruled out. The $NbO_x/Mg_xNb_yO_{x\ +\ y}$/Nb interface, fractures, and the modified electronic structure of rock salt phase may all contribute the high H_2 diffusion/surface interaction in the system. A widely accepted similar mechanism was earlier proposed by Wallace et al. for $LaNi_5$ intermetallic hydride (Wallace et al. 1979).

5.4.3 *Reactive Hydride Composites, Amide/Imides, and Other High-Capacity Systems*

An oxide composition with a specific stoichiometry may be catalytically active for various metal hydride systems, but the mechanism of dehydrogenation through additive-host interaction is not necessarily the same for each system. For example, $LiTi_2O_4$ additive is found to be effective for improving the dehydrogenation of both MgH_2, $LiAlH_4$ and $LiNH_2$ + LiH systems, but the mechanism is believed to be substantially different for each system (Zhang et al. 2014b). It was reported by Zheng et al. that the crystal structure of $LiTi_2O_4$ additive play a key role in enhancing the H ab-/desorption kinetics of $LiNH_2$ + LiH hydrogen storage system. Since the diffusion rate of Li cations is high (108 cm^2/s) for $LiTi_2O_4$ spinal structure (Johnson 1964), its admixing with $LiNH_2$ + LiH is expected to assist the overall cationic mobility (Li^+) under lower temperatures. This "mobile" effect may apparently influence the hydrogen transport within the solid-state admixture. The authors did not comment whether the same holds true for $LiAlH_4$ and MgH_2. Particularly for MgH_2, since it is categorically a different hydride, further studies are necessary to ascertain whether the cationic mobility within the crystal structure of the additive provide bond breaking/making effects.

Chemical transformation of additive was suggested to be a main cause of catalysis in some cases. Recently, Puszkiel et al. (2017) employed lithiated titania (Li_xTiO_2) as additive for the promising reactive hydride composite (RHC), $2LiBH_4 + MgH_2$. In this case, the additive plays a key role in "reaction route modification" that results to equilibrium condition at shorter reaction time. Note that $LiBH_4$ is an irreversible complex hydride that releases hydrogen through the following reaction (ΔH=75 kJ/mol H_2):

$$LiBH_4 \rightarrow LiH + B + 1.5H_2 \tag{5.10}$$

In order to restore $LiBH_4$, the LiH + B mixture requires to be placed under a hydrogen atmosphere at 600 °C and 350 bar pressure. Hence, $LiBH_4$ is generally categorized as an irreversible hydride. However, when $LiBH_4$ is reacted with MgH_2 in 2:1 molar ratio, a reversible reaction occurs as shown in (5.11):

$$2LiBH_4 + MgH_2 \rightarrow 2LiH + MgB_2 + 4H_2 \tag{5.11}$$

This RHC reaction exhibits enthalpy 46 kJ/mol.H_2 with a theoretical hydrogen capacity of 11.4 wt%, which is 29 kJ/mol.H_2 lower in comparison with pure $LiBH_4$. However, under standard reaction conditions with a few bars of overpressure, instead of evolving to MgB_2, the decomposition of $LiBH_4$ and MgH_2 occurs separately with the imminent formation of unintended intermediate products. For example, at 400–450 °C with an overpressure of 3–5 bar pressure, initially, MgH_2 decomposes to Mg and H_2. $LiBH_4$ proceeds with an unintended slow kinetic intermediate reaction (5.12) before ending with reaction products as given in (5.11),

$$2LiBH_4 \rightarrow (1/6)Li_2B_{12}H_{12} + (5/3)LiH + (13/6)H_2 \tag{5.12}$$

A few researchers suggest that the $Li_2B_{12}H_{12}$ formation can be suppressed by making the reaction at pressure higher than 10 bar. On the other hand, lithiated TiO_2 (Li_xTiO_2) additive loaded RHC proceeds to reaction (5.11) at low back pressures (3 bar) without any signs of $Li_2B_{12}H_{12}$ intermediate in the reaction. An experimental evidence indicating the modification of reaction route when adding lithiated titania additive with $LiBH_4/MgB_2$ RHC is demonstrated by Fig. 5.10. The profiles (a) and (b), respectively, show the isothermal dehydrogenation kinetics recorded at 425 °C at 3 bar H_2 pressure (temperature program: heating with 10 °C/min to the target temperature). As seen, in the RHC sample that contains no additive, among the total capacity (11.4 wt.%, normalized in the figure), about 60–70% is liberated in the first step with fast kinetics, whereas the remaining hydrogen releases with very slow kinetics. On the other hand, in the lithiated titania loaded RHC sample, among the total hydrogen capacity (8 wt.%, normalized in the figure), although about a 20% is released during heating the sample (probably due to a premature release from MgH_2 but is usually expected), comparatively a much better kinetics can be achieved. When samples taken from two different stages of desorption (marked in the figure) were tested by Raman spectroscopy, the existence of $Li_2B_{12}H_{12}$ complex can be

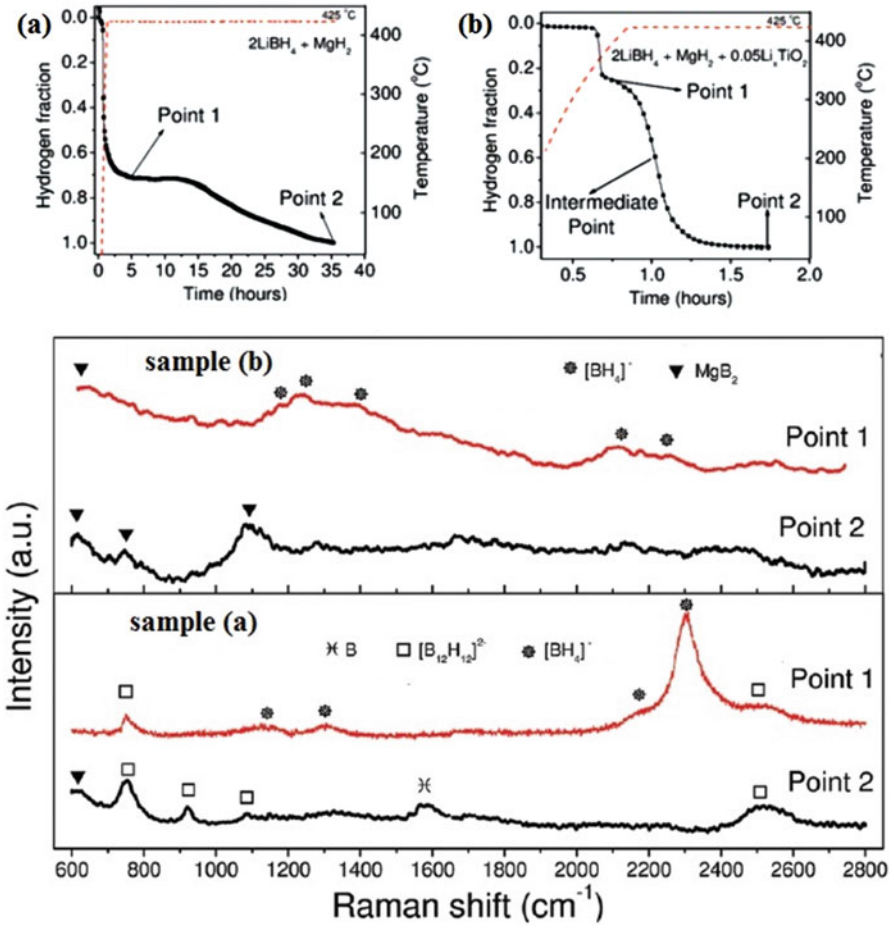

Fig. 5.10 (**a**) Isothermal dehydrogenation kinetics at 425 °C/3 bar H_2 pressure for $2LiBH_4$+MgH_2 sample, (**b**) kinetics at 425 °C/3 bar H_2 pressure for $2LiBH_4 + MgH_2 + 0.5Li_xTiO_2$ sample, (**c**) Raman spectra of both samples "a" and "b" taken from two reaction stages (marked as point 1/point 2 in both samples). (Adopted with permission from Puszkiel et al. 2017 Copyright © 2017, Royal Society of Chemistry)

proved only in the additive-free RHC sample (taken at state 2 of the sample). The Raman spectral data shown in Fig. 5.10 further reveals that transformation of boron atoms from $[BH_4]^-$ complex to make MgB_2 occurs only in the additive loaded sample under identical experimental conditions. Further studies reveal that when a 5 mol.% lithiated titania ($Li_{0.59}TiO_2$) admixed $2LiBH_4 + MgH_2$ is dehydrogenated, the additive initially reacts with $LiBH_4$ as shown in (5.13),

$$LiBH_4 + Li_{0.59}TiO_2 \rightarrow LiTiO_2 + 0.59LiH + B + 1.705H_2 \quad (5.13)$$

Subsequently, formation of MgB_2 seeds occurs from the partly decomposed Mg and B, and it defies the formation of $Li_2B_{12}H_{12}$ intermediate. The MgB_2 seeds provide coherent interfaces to promote the heterogeneous nucleation and the further growth of hexagonal MgB_2. Interestingly, apart from contributing the formation of MgB_2, the additive also contributes for the formation of LiH through reaction (5.14).

$$LiTiO_2 + 0.205H_2 \rightarrow Li_{0.59}TiO_2 + 0.41LiH. \quad (5.14)$$

When the MgB_2+LiH mixture is hydrogenated, formation of $LiTiO_2$ occurs again. The entire reaction system in the above experiments suggest that when $Li_{0.59}TiO_2$ additive was incorporated with the $2LiBH_4$+MgH_2 composite, the additive undergoes a chemical transformation and reversibly mediates the entire reaction by suppressing the undesired reaction products. Note that there were metals, chlorides, fluorides, and various other classes of materials tested for $2LiBH_4$+MgH_2 and it would be interesting to know how different the reaction mechanism of those systems are in contrast with the lithiated titania. Extensive theoretical investigations focused to extracting the transition states and the corresponding energetics will give interesting clues to understand the generalized mechanism of RHC reaction (5.11) improved by additives.

In another work, Fan et al. (2008) used Nb_2O_5 additive for catalyzing the RHC reaction (5.11) and observed that Nb_2O_5 transforms to NbH_2, initially during ball milling the $LiBH_4$/MgH_2 with Nb_2O_5 additive and subsequently by the dehydrogenation experiment. In this case a temperature reduction of at least 50 °C with significantly improved kinetics was reported, and there was no identification of intermediate phase(s) during the desorption measurements. Moreover, the product forms the RHC again, and the NbH_2 remains without further chemical modification. It obviously suggests that the way Nb_2O_5 catalyzes the RHC is different as compared to lithiated titania discussed above, but the role seems to be suppressing the intermediate phase(s). Reports in the literature suggest that $LiBH_4$ itself can be separately catalyzed by metal oxide additives for low-temperature hydrogen release. In this case the catalytic reaction is found to be redox-type chemical reaction, as depicted by $LiBH_4$+$MO_x \rightarrow LiMO_x$+B+$2H_2$ (Yu et al. 2009). Nonetheless, the reaction is not reversible, and addition of MgH_2 is necessary for driving reversibility.

Another distinct example regarding the superior role of metal oxides as additives is the catalytically enhanced hydrogen evolution reaction in ammonia borane (AB) system (Bluhm et al. 2006). Ammonia borane is known as an irreversible high-capacity hydrogen storage system (hydrogen capacity, 20 wt.%). In order to release hydrogen from AB, one has to either thermally decompose it (thermolysis) or react it with water (hydrolysis). In the process of thermolysis, hydrogen is liberated in three steps at temperatures 100 °C, 150 °C, and 500 °C. By hydrolysis on the other hand, desorption can be achieved at lower temperatures, but the reaction kinetics is poor (<1 wt.%/day) due to high activation barriers. Lapin and D'yankova (Lapin and

D'yankova 2013) showed that oxides of certain metals, especially Co_3O_4 substantially decrease the activation energy barrier from 100 kJ/mol.H_2 to 48 kJ/mol.H_2. The authors tested a number of metal oxide additives and noted that the catalytic activity of ZnO, CdO, TiO_2, MnO_2, Cr_2O_3, and WO_3 is negligible whereas Cu_2O, CuO, MoO_3, V_2O_5, Co_3O_4, and $Fe_2O_3.nH_2O$ yield moderate improvement. These observations suggest that an active oxide additive known for one metal hydride may be passive for another metal hydride.

Lithium amide/imide is another promising hydrogen storage system for which metal oxides were proven to be effective for improving the reaction kinetics (Zhang et al. 2014a). Chen et al. was the first to report that lithium nitride (Li_3N) absorbs 10.4 wt.% of hydrogen reversibly (Chen et al. 2002) through a two-step reaction as shown in (5.15) and (5.16).

$$Li_3N + H_2 \leftrightarrow Li_2NH + LiH \tag{5.15}$$

$$Li_2NH + H_2 \leftrightarrow LiNH_2 + LiH \tag{5.16}$$

The enthalpy of these two reactions, respectively, −165 kJ/mol.H_2 and −44.55 kJ/mol.H_2. Due to the low enthalpy, only the second reaction (capacity, 6.5 wt.%) is considered viable for hydrogen storage applications. However, one of the important issues is that usually $LiNH_2$ releases ammonia at 300 °C by following reaction (5.17).

$$2LiNH_2 \rightarrow Li_2NH + NH_3 \tag{5.17}$$

Lchikawa et al. (Ichikawa et al. 2004) showed that the release of NH_3 depends on how intimately LiH binds with $LiNH_2$. The poorly bound powder releases ammonia as per reaction (5.17), whereas the closely bound mixture releases hydrogen as per reaction (5.16). Therefore, one of the important roles of additive in this case is believed to be shielding the reactants so as to offer a better surface contact.

Later developments in lithium amide hydrogen storage system suggested that Li can be substituted by Mg and better performance and higher capacity can be achieved (Janot et al. 2007; Li et al. 2014). For further understanding regarding the hydrogen storage aspects of amide-imide systems, the reader is directed to references (David et al. 2007; Miwa et al. 2005). The work of Anton et al. (2011) on MgH_2 + $LiNH_2$ hydrogen storage system identified that by incorporation of defects through ball milling, the release of ammonia can be controlled and better reaction kinetics can be achieved. When the additives V_2O_5 and Fe_2O_3 were employed, the authors observed controlled release of ammonia and faster kinetics. From these observations, it was concluded that the role of oxide additives is to incorporate more defects in the system. Yuan et al. (2012) employed various metal oxide nanoparticle additives such as CeO_2, TiO_2, Fe_2O_3, Co_3O_4, and SiO_2 for improving the hydrogen storage performance of another mixed hydride system $LiBH_4/2LiNH_2/MgH_2$. Based upon the improved desorption performance, they

have categorized the catalytic activity with a series, $Fe_2O_3 > Co_3O_4 > CeO_2 > TiO_2 > SiO_2$.

Numerous examples are available in the literature regarding the superior effect of metal oxides as additives for many other hydrogen storage materials. For further information, the reader is directed to material specific journal articles regularly updated in the literature.

5.5 Summary and Outlook

The above discussions suggest that the best metal oxide additive known for one metal hydride is not necessarily a best for another hydride and also the additive-hydride interaction cannot be generalized. Likewise, for a particular metal hydride, many oxide additives may be proven active, but the interaction need not remain the same. However, since bond breaking/making is the end result of each catalytic reaction, catalytically enhanced common bonding/antibonding mechanism do exist, and it should be well understood for optimizing any system for commercial applications. In this connection, for understanding the catalytic mechanism, the details regarding how a hydride chemically interacts with various oxide additives should be well studied. In the literature, by performing comparative studies, researchers categorize the effectiveness of oxide additives from most effective to least effective. On many occasions, whereas extensive characterization studies are performed on the most effective oxide additive, the least effective oxides are ignored without further scrutiny. Nonetheless, it is also necessary to identify what makes an additive least effective for formulating a general catalytic mechanism for the system. Moreover, note that any comparison of additives made in the literature without taking into account the size effect may not be accurate. There are materials known to be less active in bulk scale that become very active when scaled down to nano-order. This suggests that any comparative studies reported in the literature with no reference to size effects may have erroneous conclusions. As we decrease the size of the particles, the number of atoms in direct chemical contact with the surrounding species increases significantly. Apart from this, in the case of metal oxides, the exposed atoms in the surface usually do not reflect the correct stoichiometry of the compound as the surface cation/anion ratio is significantly different as compared to the overall ionic ratio and bulk stoichiometry. The distinct valence states and vacancies existing at the surface of oxide nanoparticles substantially influence their chemical proximity as compared to the bulk structure. When two non-reducible oxide samples with the same size and chemical composition but exhibiting different crystal structure are used as additives for a hydride, the result may not remain the same, because the surface cation/anion ratio is different for different crystal structures. Considering all these aspects, in order to understand the mechanism of a catalytic reaction, it is necessary to correctly test the interaction of various metal oxides with a hydride and understand what common observation connects all these oxides. Such a study will be helpful for making a generalized

mechanism for understanding catalytically improved reactions. In this connection, the interesting literature data supports compiled in this chapter may guide readers for understanding the various possibilities of additive-hydride interaction.

5.6 Conclusions

The additives that catalyze a metal hydride by making in situ catalysts through a chemical reaction with the hydride are the most suitable for high enthalpy hydrides. Due to the formation of in situ catalyst, tuning the thermodynamics of the hydride is likely, at least a small extent. Maintaining the stability of the in situ catalysts is one challenge presently, but further research in this direction will bring revolutions for sustainable energy development.

References

Aguey-Zinsou KF, Ares Fernandez JR, Klassen T, Bormann R (2007) Effect of Nb2O5 on MgH2 properties during mechanical milling. Int J Hydrog Energy 32:2400–2407. https://doi.org/10.1016/j.ijhydene.2006.10.068

Anton DL, Price CJ, Gray J (2011) Affects of mechanical milling and metal oxide additives on sorption kinetics of 1:1 LiNH2/MgH2 mixture. Energies 4:826

Barkhordarian G, Klassen T, Bormann R (2003) Fast hydrogen sorption kinetics of nanocrystalline Mg using Nb2O5 as catalyst. Scr Mater 49:213–217. https://doi.org/10.1016/S1359-6462(03)00259-8

Bluhm ME, Bradley MG, Butterick R, Kusari U, Sneddon LG (2006) Amineborane-based chemical hydrogen storage: enhanced ammonia borane dehydrogenation in ionic liquids. J Am Chem Soc 128:7748–7749. https://doi.org/10.1021/ja062085v

Bogdanović B, Sandrock G (2011) Catalyzed complex metal hydrides. MRS Bull 27:712–716. https://doi.org/10.1557/mrs2002.227

Bogdanović B et al (2003) Investigation of hydrogen discharging and recharging processes of Ti-doped NaAlH4 by X-ray diffraction analysis (XRD) and solid-state NMR spectroscopy. J Alloys Compd 350:246–255. https://doi.org/10.1016/S0925-8388(02)00953-2

Bogdanović B, Eberle U, Felderhoff M, Schüth F (2007) Complex aluminum hydrides. Scr Mater 56:813–816. https://doi.org/10.1016/j.scriptamat.2007.01.004

Borgschulte A, Bielmann M, Züttel A, Barkhordarian G, Dornheim M, Bormann R (2008) Hydrogen dissociation on oxide covered MgH2 by catalytically active vacancies. Appl Surf Sci 254:2377–2384. https://doi.org/10.1016/j.apsusc.2007.09.069

Bruce PG, Scrosati B, Tarascon JM (2008) Nanomaterials for rechargeable lithium batteries. Angew Chem Int Ed 47:2930–2946. https://doi.org/10.1002/anie.200702505

Cao G (2004) Nanostructures & nanomaterials: synthesis, properties & applications. Imperial College Press, London

Chen X, Mao SS (2007) Titanium dioxide nanomaterials: synthesis, properties, modifications, and applications. Chem Rev 107:2891–2959. https://doi.org/10.1021/cr0500535

Chen P, Xiong Z, Luo J, Lin J, Tan KL (2002) Interaction of hydrogen with metal nitrides and imides. Nature 420:302. https://doi.org/10.1038/nature01210 https://www.nature.com/articles/nature01210#supplementary-information

Cho ES, Ruminski AM, Aloni S, Liu Y-S, Guo J, Urban JJ (2016) Graphene oxide/metal nanocrystal multilaminates as the atomic limit for safe and selective hydrogen storage. Nat Commun 7:10804. https://doi.org/10.1038/ncomms10804 https://www.nature.com/articles/ncomms10804#supplementary-information

Croston DL, Grant DM, Walker GS (2010) The catalytic effect of titanium oxide based additives on the dehydrogenation and hydrogenation of milled MgH2. J Alloys Compd 492:251–258. https://doi.org/10.1016/j.jallcom.2009.10.199

Daniel M-C, Astruc D (2004) Gold nanoparticles: assembly, supramolecular chemistry, quantum-size-related properties, and applications toward biology, catalysis, and nanotechnology. Chem Rev 104:293–346. https://doi.org/10.1021/cr030698+

David WIF, Jones MO, Gregory DH, Jewell CM, Johnson SR, Walton A, Edwards PP (2007) A mechanism for non-stoichiometry in the lithium amide/lithium imide hydrogen storage reaction. J Am Chem Soc 129:1594–1601. https://doi.org/10.1021/ja066016s

Eustis S, El-Sayed MA (2006) Why gold nanoparticles are more precious than pretty gold: noble metal surface plasmon resonance and its enhancement of the radiative and nonradiative properties of nanocrystals of different shapes. Chem Soc Rev 35:209–217. https://doi.org/10.1039/B514191E

Fan M-Q, Sun L-X, Zhang Y, Xu F, Zhang J, H-l C (2008) The catalytic effect of additive Nb2O5 on the reversible hydrogen storage performances of LiBH4–MgH2 composite. Int J Hydrog Energy 33:74–80. https://doi.org/10.1016/j.ijhydene.2007.09.012

Felderhoff M et al (2004) Combined TEM-EDX and XAFS studies of Ti-doped sodium alanate. Phys Chem Chem Phys 6:4369–4374. https://doi.org/10.1039/B403657N

Fichtner M, Fuhr O, Kircher O, Rothe J (2003) Small Ti clusters for catalysis of hydrogen exchange in NaAlH4. Nanotechnology 14:778

Friedrichs O, Klassen T, Sánchez-López JC, Bormann R, Fernández A (2006a) Hydrogen sorption improvement of nanocrystalline MgH2 by Nb2O5 nanoparticles. Scr Mater 54:1293–1297. https://doi.org/10.1016/j.scriptamat.2005.12.011

Friedrichs O, Sánchez-López JC, López-Cartes C, Dornheim M, Klassen T, Bormann R, Fernández A (2006b) Chemical and microstructural study of the oxygen passivation behaviour of nanocrystalline Mg and MgH2. Appl Surf Sci 252:2334–2345. https://doi.org/10.1016/j.apsusc.2005.04.018

Friedrichs O et al (2006c) MgH2 with Nb2O5 as additive, for hydrogen storage: chemical, structural and kinetic behavior with heating. Acta Mater 54:105–110. https://doi.org/10.1016/j.actamat.2005.08.024

Friedrichs O, Martínez-Martínez D, Guilera G, Sánchez López JC, Fernández A (2007) In situ energy-dispersive XAS and XRD study of the superior hydrogen storage system MgH2/Nb2O5. J Phys Chem C 111:10700–10706. https://doi.org/10.1021/jp0675835

Gawande MB, Pandey RK, Jayaram RV (2012) Role of mixed metal oxides in catalysis science-versatile applications in organic synthesis. Cat Sci Technol 2:1113–1125. https://doi.org/10.1039/C2CY00490A

Hanada N, Ichikawa T, Fujii H (2005) Catalytic effect of Ni nano-particle and Nb oxide on H-desorption properties in MgH2 prepared by ball milling. J Alloys Compd 404–406:716–719. https://doi.org/10.1016/j.jallcom.2004.12.166

Hanada N et al (2009) X-ray absorption spectroscopic study on valence state and local atomic structure of transition metal oxides doped in MgH2. J Phys Chem C 113:13450–13455. https://doi.org/10.1021/jp901859f

Handelman A, Beker P, Amdursky N, Rosenman G (2012) Physics and engineering of peptide supramolecular nanostructures. Phys Chem Chem Phys 14:6391–6408. https://doi.org/10.1039/c2cp40157f

Haruta M (2002) Catalysis of gold nanoparticles deposited on metal oxides. Cattech 6:102–115

Henrich VE, Cox PA (1996) The surface science of metal oxides. Cambridge university press, Cambridge

Huang ZG, Guo ZP, Calka A, Wexler D, Lukey C, Liu HK (2006) Effects of iron oxide (Fe2O3, Fe3O4) on hydrogen storage properties of Mg-based composites. J Alloys Compd 422:299–304. https://doi.org/10.1016/j.jallcom.2005.11.074

Ichikawa T, Isobe S, Hanada N, Fujii H (2004) Lithium nitride for reversible hydrogen storage. J Alloys Compd 365:271–276. https://doi.org/10.1016/S0925-8388(03)00637-6

Janot R, Eymery J-B, Tarascon J-M (2007) Investigation of the processes for reversible hydrogen storage in the Li–Mg–N–H system. J Power Sources 164:496–502. https://doi.org/10.1016/j.jpowsour.2006.11.046

Jeon K-J, Moon HR, Ruminski AM, Jiang B, Kisielowski C, Bardhan R, Urban JJ (2011) Air-stable magnesium nanocomposites provide rapid and high-capacity hydrogen storage without using heavy-metal catalysts. Nat Mater 10:286. https://doi.org/10.1038/nmat2978 https://www.nature.com/articles/nmat2978#supplementary-information

Johnson OW (1964) One-dimensional diffusion of Li in rutile. Phys Rev 136:A284–A290

Jung KS, Lee EY, Lee KS (2006) Catalytic effects of metal oxide on hydrogen absorption of magnesium metal hydride. J Alloys Compd 421:179–184. https://doi.org/10.1016/j.jallcom.2005.09.085

Kalidindi SB, Jagirdar BR (2009) Highly monodisperse colloidal magnesium nanoparticles by room temperature digestive ripening. Inorg Chem 48:4524–4529. https://doi.org/10.1021/ic9003577

Kelly KL, Coronado E, Zhao LL, Schatz GC (2003) The optical properties of metal nanoparticles: the influence of size, shape, and dielectric environment. J Phys Chem B 107:668–677. https://doi.org/10.1021/jp026731y

Kim HW et al (2013) Selective gas transport through few-layered graphene and graphene oxide membranes. Science 342:91

Kobayashi H, Salahub DR, Ito T (1994) Dissociative adsorption of hydrogen molecule on MgO surfaces studied by the density functional method. J Phys Chem 98:5487–5492. https://doi.org/10.1021/j100072a015

Kung HH (1989) Transition metal oxides: surface chemistry and catalysis, vol 45. Elsevier, Amsterdam

Lapin NV, D'yankova NY (2013) Hydrogen evolution kinetics during transition metal oxide-catalyzed ammonia borane hydrolysis. Inorg Mater 49:975–979. https://doi.org/10.1134/s0020168513100063

Lee G-J, Kim JW, Shim J-H, Cho YW, Lee KS (2007a) Synthesis of ultrafine titanium aluminide powders and their catalytic enhancement in dehydrogenation kinetics of NaAlH4. Scr Mater 56:125–128. https://doi.org/10.1016/j.scriptamat.2006.09.027

Lee G-J, Shim J-H, Whan Cho Y, Sub Lee K (2007b) Reversible hydrogen storage in NaAlH4 catalyzed with lanthanide oxides. Int J Hydrog Energy 32:1911–1915. https://doi.org/10.1016/j.ijhydene.2006.10.023

Lee G-J, Shim J-H, Cho YW, Lee KS (2008) Improvement in desorption kinetics of NaAlH4 catalyzed with TiO2 nanopowder. Int J Hydrog Energy 33:3748–3753. https://doi.org/10.1016/j.ijhydene.2008.04.035

Léon A, Kircher O, Rothe J, Fichtner M (2004) Chemical state and local structure around titanium atoms in NaAlH4 doped with TiCl3 using x-ray absorption spectroscopy. J Phys Chem B 108:16372–16376. https://doi.org/10.1021/jp048615w

Li P, Li Z, Zhai F, Wan Q, Li X, Qu X, Volinsky AA (2013) NiFe2O4 nanoparticles catalytic effects of improving LiAlH4 dehydrogenation properties. J Phys Chem C 117:25917–25925. https://doi.org/10.1021/jp408364p

Li C, Liu Y, Ma R, Zhang X, Li Y, Gao M, Pan H (2014) Superior dehydrogenation/hydrogenation kinetics and long-term cycling performance of K and Rb Cocatalyzed Mg(NH2)2-2LiH system. ACS Appl Mater Interfaces 6:17024–17033. https://doi.org/10.1021/am504592x

Ma J, Li J, Tang RY, Li WZ, Chen QY (2012) Effects of porous Al_2O_3/SiO_2 on hydrogen storage capacities of NaAlH_4-Tm_2O_3 system [J]. Chin J Nonferrous Met 6:017

Ma T, Isobe S, Wang Y, Hashimoto N, Ohnuki S (2013) Nb-gateway for hydrogen desorption in Nb2O5 catalyzed MgH2 nanocomposite. J Phys Chem C 117:10302–10307. https://doi.org/10.1021/jp4021883

Majzoub EH, Gross KJ (2003) Titanium–halide catalyst-precursors in sodium aluminum hydrides. J Alloys Compd 356–357:363–367. https://doi.org/10.1016/S0925-8388(03)00113-0

Miwa K, Ohba N, Towata S-i, Nakamori Y, Orimo S-i (2005) First-principles study on lithium amide for hydrogen storage. Phys Rev B 71:195109

Morioka H, Kakizaki K, Chung S-C, Yamada A (2003) Reversible hydrogen decomposition of KAlH4. J Alloys Compd 353:310–314. https://doi.org/10.1016/S0925-8388(02)01307-5

Nielsen TK, Jensen TR (2012) MgH2–Nb2O5 investigated by in situ synchrotron X-ray diffraction. Int J Hydrog Energy 37:13409–13416. https://doi.org/10.1016/j.ijhydene.2012.06.082

Norris DJ, Bawendi M (1996) Measurement and assignment of the size-dependent optical spectrum in CdSe quantum dots. Phys Rev B 53:16338

Oelerich W, Klassen T, Bormann R (2001a) Comparison of the catalytic effects of V, V2O5, VN, and VC on the hydrogen sorption of nanocrystalline Mg. J Alloys Compd 322:L5–L9. https://doi.org/10.1016/S0925-8388(01)01173-2

Oelerich W, Klassen T, Bormann R (2001b) Metal oxides as catalysts for improved hydrogen sorption in nanocrystalline Mg-based materials. J Alloys Compd 315:237–242. https://doi.org/10.1016/S0925-8388(00)01284-6

Orimo S-i, Nakamori Y, Eliseo JR, Züttel A, Jensen CM (2007) Complex hydrides for hydrogen storage. Chem Rev 107:4111–4132. https://doi.org/10.1021/cr0501846

Patah A, Takasaki A, Szmyd JS (2009) Influence of multiple oxide (Cr2O3/Nb2O5) addition on the sorption kinetics of MgH2. Int J Hydrog Energy 34:3032–3037. https://doi.org/10.1016/j.ijhydene.2009.01.086

Polanski M, Bystrzycki J (2009) Comparative studies of the influence of different nano-sized metal oxides on the hydrogen sorption properties of magnesium hydride. J Alloys Compd 486:697–701. https://doi.org/10.1016/j.jallcom.2009.07.042

Polanski M, Bystrzycki J, Varin RA, Plocinski T, Pisarek M (2011) The effect of chromium (III) oxide (Cr2O3) nanopowder on the microstructure and cyclic hydrogen storage behavior of magnesium hydride (MgH2). J Alloys Compd 509:2386–2391. https://doi.org/10.1016/j.jallcom.2010.11.026

Porcu M, Petford-Long AK, Sykes JM (2008) TEM studies of Nb2O5 catalyst in ball-milled MgH2 for hydrogen storage. J Alloys Compd 453:341–346. https://doi.org/10.1016/j.jallcom.2006.11.147

Pukazhselvan D (2012) Effect of crystallite size of Al on the reversible hydrogen storage of NaAlH4 and few aspects of catalysts and catalysis. Int J Hydrog Energy 37:9696–9705. https://doi.org/10.1016/j.ijhydene.2012.03.098

Pukazhselvan D, Hudson MSL, Sinha ASK, Srivastava ON (2010) Studies on metal oxide nanoparticles catalyzed sodium aluminum hydride. Energy 35:5037–5042. https://doi.org/10.1016/j.energy.2010.08.015

Pukazhselvan D, Kumar V, Singh SK (2012) High capacity hydrogen storage: basic aspects, new developments and milestones. Nano Energy 1:566–589. https://doi.org/10.1016/j.nanoen.2012.05.004

Pukazhselvan D, Antunes I, Lo Russo S, Perez J, Fagg DP (2014a) Synthesis of catalytically active rock salt structured MgxNb1−xO nanoparticles for MgH2 system. Int J Hydrog Energy 39:18984–18988. https://doi.org/10.1016/j.ijhydene.2014.08.138

Pukazhselvan D, Capurso G, Maddalena A, Lo Russo S, Fagg DP (2014b) Hydrogen storage characteristics of magnesium impregnated on the porous channels of activated charcoal scaffold. Int J Hydrog Energy 39:20045–20053. https://doi.org/10.1016/j.ijhydene.2014.10.038

Pukazhselvan D, Fagg DP, Srivastava ON (2015) One step high pressure mechanochemical synthesis of reversible alanates NaAlH4 and KAlH4. Int J Hydrog Energy 40:4916–4924. https://doi.org/10.1016/j.ijhydene.2015.01.186

Pukazhselvan D, Bdikin I, Perez J, Carbó-Argibay E, Antunes I, Stroppa DG, Fagg DP (2016a) Formation of Mg–Nb–O rock salt structures in a series of mechanochemically activated MgH2 + nNb2O5 (n = 0.083–1.50) mixtures. Int J Hydrog Energy 41:2677–2688. https://doi.org/10.1016/j.ijhydene.2015.12.077

Pukazhselvan D, Nasani N, Pérez J, Hortigüela MJ, Yang T, Bdikin I, Fagg DP (2016b) Two step mechanochemical synthesis of Nb doped MgO rock salt nanoparticles and its application for hydrogen storage in MgH2. Int J Hydrog Energy 41:11716–11722. https://doi.org/10.1016/j.ijhydene.2015.11.175

Pukazhselvan D, Otero-Irurueta G, Pérez J, Singh B, Bdikin I, Singh MK, Fagg DP (2016c) Crystal structure, phase stoichiometry and chemical environment of MgxNbyOx+y nanoparticles and their impact on hydrogen storage in MgH2. Int J Hydrog Energy 41:11709–11715. https://doi.org/10.1016/j.ijhydene.2016.04.029

Pukazhselvan D, Perez J, Nasani N, Bdikin I, Kovalevsky AV, Fagg DP (2016d) Formation of MgxNbyOx+y through the mechanochemical reaction of MgH2 and Nb2O5, and its effect on the hydrogen-storage behavior of MgH2. Chem Phys Chem 17:178–183. https://doi.org/10.1002/cphc.201500620

Pukazhselvan D, Nasani N, Correia P, Carbó-Argibay E, Otero-Irurueta G, Stroppa DG, Fagg DP (2017a) Evolution of reduced Ti containing phase(s) in MgH2/TiO2 system and its effect on the hydrogen storage behavior of MgH2. J Power Sources 362:174–183. https://doi.org/10.1016/j.jpowsour.2017.07.032

Pukazhselvan D, Nasani N, Sandhya KS, Singh B, Bdikin I, Koga N, Fagg DP (2017b) Role of chemical interaction between MgH2 and TiO2 additive on the hydrogen storage behavior of MgH2. Appl Surf Sci 420:740–745. https://doi.org/10.1016/j.apsusc.2017.05.182

Puszkiel JA et al (2017) Changing the dehydrogenation pathway of LiBH4-MgH2via nanosized lithiated TiO2. Phys Chem Chem Phys 19:7455–7460. https://doi.org/10.1039/C6CP08278E

Rafi ud d, Xuanhui Q, Ping L, Zhang L, Ahmad M (2011) Hydrogen sorption improvement of LiAlH4 catalyzed by Nb2O5 and Cr2O3 nanoparticles. J Phys Chem C 115:13088–13099. https://doi.org/10.1021/jp202969y

Rafi ud d et al (2012) Superior catalytic effects of Nb2O5, TiO2, and Cr2O3 nanoparticles in improving the hydrogen sorption properties of NaAlH4. J Phys Chem C 116:11924–11938. https://doi.org/10.1021/jp302474c

Rahman MW, Livraghi S, Dolci F, Baricco M, Giamello E (2011) Hydrogen sorption properties of Ternary Mg–Nb–O phases synthesized by solid–state reaction. Int J Hydrog Energy 36:7932–7936. https://doi.org/10.1016/j.ijhydene.2011.01.053

Sadhasivam T, Sterlin Leo Hudson M, Pandey SK, Bhatnagar A, Singh MK, Gurunathan K, Srivastava ON (2013) Effects of nano size mischmetal and its oxide on improving the hydrogen sorption behaviour of MgH2. Int J Hydrog Energy 38:7353–7362. https://doi.org/10.1016/j.ijhydene.2013.04.040

Sandhya KS, Pukazhselvan D, Fagg DP, Koga N (2016) Interaction of magnesium hydride clusters with Nb doped MgO additive studied by density functional calculations. RSC Adv 6:61200–61206. https://doi.org/10.1039/C6RA11281A

Sapra S, Sarma DD (2004) Evolution of the electronic structure with size in II-VI semiconductor nanocrystals. Phys Rev B 69:125304

Schlapbach L (1981) XPS/UPS study of the oxidation of La and LaNi5 and of the electronic structure of LaNi5. Solid State Commun 38:117–123. https://doi.org/10.1016/0038-1098(81)90802-4

Schoenitz M, Zhu X, Dreizin EL (2004) Mechanical alloys in the Al-rich part of the Al-Ti binary system. J Metastable Nanocryst Mater 20–21, 455–461. Trans Tech Publ

Schwarz JA, Contescu CI, Putyera K (2004) Dekker encyclopedia of nanoscience and nanotechnology, vol 3. CRC press, Boca Raton

Wallace WE, Karlicek RF, Imamura H (1979) Mechanism of hydrogen absorption by lanthanum-nickel (LaNi5). J Phys Chem 83:1708–1712. https://doi.org/10.1021/j100476a006

Wan LF et al (2017) Atomically thin interfacial suboxide key to hydrogen storage performance enhancements of magnesium nanoparticles encapsulated in reduced graphene oxide. Nano Lett 17:5540–5545. https://doi.org/10.1021/acs.nanolett.7b02280

Weaver JH, Franciosi A, Wallace WE, Smith HK (1980) Electronic structure and surface oxidation of LaNi5, Er6Mn23, and related systems. J Appl Phys 51:5847–5851. https://doi.org/10.1063/1.327544

Wu G, Zhang J, Wu Y, Li Q, Chou K, Bao X (2009) Adsorption and dissociation of hydrogen on MgO surface: a first-principles study. J Alloys Compd 480:788–793. https://doi.org/10.1016/j.jallcom.2009.02.086

Yu PY, Cardona M (1996) Fundamentals of semiconductors: physics and materials properties. Springer, Heidelberg

Yu XB, Grant DM, Walker GS (2009) Dehydrogenation of LiBH4 destabilized with various oxides. J Phys Chem C 113:17945–17949. https://doi.org/10.1021/jp906519p

Yuan H et al (2012) Influence of metal oxide on LiBH4/2LiNH2/MgH2 system for hydrogen storage properties. Int J Hydrog Energy 37:3292–3297. https://doi.org/10.1016/j.ijhydene.2011.11.065

Yuan C, Wu HB, Xie Y, Lou XW (2014) Mixed transition-metal oxides: design, synthesis, and energy-related applications. Angew Chem Int Ed 53:1488–1504. https://doi.org/10.1002/anie.201303971

Zaluska A, Zaluski L, Ström-Olsen J (2001) Structure, catalysis and atomic reactions on the nano-scale: a systematic approach to metal hydrides for hydrogen storage. Appl Phys A 72:157–165

Zaluski L, Zaluska A, Ström-Olsen JO (1997) Nanocrystalline metal hydrides. J Alloys Compd 253–254:70–79. https://doi.org/10.1016/S0925-8388(96)02985-4

Zhang M, Li J, Li H, Li Y, Shen W (2009) Morphology-dependent redox and catalytic properties of CeO2 nanostructures: nanowires, nanorods and nanoparticles. Catal Today 148:179–183

Zhang T, Isobe S, Wang Y, Hashimoto N, Ohnuki S (2014a) A homogeneous metal oxide catalyst enhanced solid–solid reaction in the hydrogen desorption of a lithium–hydrogen–nitrogen system. ChemCatChem 6:724–727. https://doi.org/10.1002/cctc.201301068

Zhang T, Isobe S, Wang Y, Oka H, Hashimoto N, Ohnuki S (2014b) A metal-oxide catalyst enhanced the desorption properties in complex metal hydrides. J Mater Chem A 2:4361–4365. https://doi.org/10.1039/C3TA15294D

Zhao-Karger Z, Hu J, Roth A, Wang D, Kubel C, Lohstroh W, Fichtner M (2010) Altered thermodynamic and kinetic properties of MgH2 infiltrated in microporous scaffold. Chem Commun 46:8353–8355. https://doi.org/10.1039/C0CC03072D

Zlotea C, Oumellal Y, Hwang S-J, Ghimbeu CM, de Jongh PE, Latroche M (2015) Ultrasmall MgH2 nanoparticles embedded in an ordered microporous carbon exhibiting rapid hydrogen sorption kinetics. J Phys Chem C 119:18091–18098. https://doi.org/10.1021/acs.jpcc.5b05754